Iran. J. Biotechnol. April 2022;20(2): e3179 DOI: 10.30498/ijb.2022.310552.3179

Research Article

Effect of Olibanum Extract/Graphene Oxide on Differentiation of Bone Marrow Mesenchymal Stem Cells into Neuron-Like Cells on Freeze Dried Scaffolds

Atefeh Shamosi [1], Elaheh Mahmoudi[2], Fatemeh Kermanian [1]*

[1]Department of Anatomy, School of Medicine, Alborz University of Medical Sciences, Karaj, Iran.
[2]Department of Mycology, School of Medicine, Alborz University of Medical Sciences, Karaj, Iran.

*Corresponding author: Fatemeh Kermanian, Department of Anatomy, School of Medicine, Alborz University of Medical Sciences, Karaj, Iran. Tel/fax: +98-263446009, E-mail: f.kermanian@abzums.ac.ir

Background: One of the challenges in using stem cells to neural repair is to induce their differentiation into neurons and lack of glial formation.

Objectives: Mesenchymal stem cells have revealed great potential for neural reorganization and renewal by taking advantage of differentiation capabilities. Here we explored the potential use of olibanum extract in freeze-dried scaffolds for induction of stem cells differentiation.

Materials and Methods: In this study, gelatin/ collagen/olibanum/ graphene oxide (GEL/COL/OL/GO) freeze-dried scaffolds were synthesized and then adult rat bone marrow mesenchymal stem cells (BMMSCs) were seeded on scaffolds. The viability of cells was evaluated using MTT test on days 1, 3 and 5. The morphology of the cells seeded on scaffolds was studied using SEM and specific protein expression detected by immunohistochemical analysis. Real-time PCR was applied to detect the expression of Chat, Pax6, Hb-9, Nestin, Islet-1, and neurofilament-H (NF-H). The data were analyzed using Tukey test and one-way ANOVA and the means difference was considered significant at $P<0.05$, $P<0.01$, and $P<0.001$.

Results: Showed that the pore size is increased in GEL/COL/OL/GO scaffolds compared with GO-free scaffolds and higher attachment and proliferation of BMMSCs on GEL/COL/OL /1.5% GO scaffolds compared to GEL/COL/OL/3% GO scaffolds. The cell viability results after 5 days of incubation showed the significant biocompatibility of GEL/COL/OL /1.5% GO freeze-dried scaffold. The results of immunohistochemical and PCR analysis revealed positive role of GEL/COL/OL/1.5% GO scaffolds in upregulation of neuron-specific markers.

Conclusion: These results reveal the great potential of GEL/COL/OL/GO scaffolds for nerve regeneration. Our data suggested that both OL extract and GO can regulate the MSCs differentiation into neurons.

Keywords: Bone marrow mesenchymal stem cells, Differentiation, Freeze-dried, Gelatin/collagen/olibanum/graphen oxide, Neurons

1. Background

Neural tissue regeneration approaches have acquired a great deal of attention due to it directly impacts all dimensions of the patient's life. Stem cells and progenitor cells have found a new viewpoint as a therapeutic candidate in regenerative medicine. These potent cells with the capacity to proliferate in vitro and the ability to develop into any somatic cell type are a suitable cell source (1). Scaffolds are one of the fundamental factors in regulating cellular development and renewal. Extracellular matrix with oriented fibers, conduits, and continuous pores are numerous types of morphology that have been indicated a significant effect on cell adhesion and differentiation. Many current fabricated scaffolds have been synthesized as biological structures of hydrogels and different

scales of fibers, with the purpose to simulate the natural matrix construction. Graphene oxide (GO), a neuronal biocompatible substance with charge transfer characteristics, has revealed promising results for cell survival *in vitro* (2). Its remarkable features such as good molecule attachment, high elasticity and suitable electrical conductivity have been attractive topics for tissue engineering applications. In recent investigations, both GO and its derivatives have been indicated as biocompatible materials for the improvement of growth and differentiation of different pluripotent cells such as induced pluripotent stem cells (iPSCs), Human Mesenchymal Stem Cells (hMSCs), and human primary adult neural stem cells (hNSCs) (1). Nerve Growth Factor (NGF) has been more effective to repair injured neurons by stimulating nerve renewal (2). The essential oils and extracts of plants Boswellia species, Olibanum (OL), can be useful for the enhancement of memory power in the natural system of medicine (Ayurveda) and India's traditional as well as Oriental Medicine and prevention of amnesia (3). It contains about 8 % volatile oil, 32 % carbohydrate, and 50 % resin (4). Anticancer, anti-inflammatory, no toxicity, no sensitization, and biocompatibility led to its application in different diseases including cancer, bronchial asthma, osteoarthritis, brain edema, ulcerative colitis, tissue engineering, etc. (5).

2. Objectives

In the current study, we intended to determine the synergistic effect of GEL/COL/OL/GO freeze-dried scaffolds on differentiation of bone marrow mesenchymal stem cells (BMMSCs) to neurons. The novelty of this research is in using the OL extract and GO in the tissue engineering scaffolds for the first time.

3. Materials and Methods

3.1. Purification of OL Extract

OL was purchased from the local market of Karaj, Iran. OL extract was purified according to Choi *et al*. Briefly, 12.5 gr. of OL powder was dissolved in 100 mL of DI water. After that, the supernatant was centrifuged at 2000 x g for 15 min and 10000 x g for 20 min. Then, it was filtered, freeze-dried at a temperature of -58 °C to prepare the water-soluble extract (6).

3.2. Preparation of Freeze-Dried Scaffolds

Acid-soluble collagen solution (Sigma, USA) with a gelatin A (Sigma, USA) concentration of 12 wt/% of the total amount of mixture were prepared (GEL/COL) (7). 1 wt% OL (6) was added to the GEL/COL mixture. Different concentration of GO (Sigma, USA) (1.5 wt% and 3 wt %) was then added and stirred for 2 h. The mixtures were then set into a freezer at -65 °C for 24 h. The frozen scaffold was placed into the freeze-dryer chamber for another 24 h at -58 °C with 0.01 bar to remove all the available waters)FD-10, Pishtaz Engineering Co. Iran). All freeze-dried scaffolds were soaked in DI water for 48 h to allow unreacted glutaraldehyde to leach out (8).

3.3. Characterization of Fabricated Scaffolds

3.3.1. Morphology Observation

The microstructural and morphological assessment (porosity, pore size and, as well as the interconnectivity of pores) of freeze-dried scaffolds were studied by scanning electron microscopy (SEM), (Hitachi SU8010, Japan) (9). The porosity was computed by calculating the fraction of the total area occupied by pores per image, whilst the average pore size was evaluated using Image J software (NIH, Bethesda, MD).

3.3.2. FTIR

Fourier Transform Infrared (FTIR) spectroscopy analysis was performed to assess the chemical bonds present in a sample. 2 mg. of the scraped scaffolds were quietly blended with 400 mg. of potassium bromide (KBr). Then the samples were investigated in the range of 400-4500 cm^{-1} (10).

3.3.3. Mechanical Compression

Compressive strength of the fabricated scaffolds (GEL/COL/OL/GO) was assessed with a tensile strength test system (Santam, STM 20, Iran) at room temperature. At least five specimens were investigated for each scaffold to determine the slope of the initial linear portion (11). Tensile strength of fabricated scaffolds was measured using ASTM D3039/A3039M standard number with 2 mm thickness.

3.3.4. Water Absorption

Scaffolds were cut, weighed, immersed in 20 mL phosphate buffered saline (PBS) for 2, 12, and 24 h. The excess surface water of swollen scaffold was eliminated with filter paper. The obtained weights of the swollen specimens were measured as following:

Water uptake (%) = [(W_s-W_d)/W_d] ×100 (1)

The weight of dry sample before immersing and the weight of swollen sample were mentioned W_d and W_s, respectively. Each swelling test was performed five times (10).

3.3.5. Degradation Test

To evaluate the in vitro degradation rate of fabricated scaffolds, a dry weight of samples (initial dry weight) was immersed in PBS (pH = 7.4) solution. At the end of each week, the specimen was freeze-dried at −58 °C for 24 h at a vacuum pressure of 0.5 Torr (dry weight). The *in vitro* degradation was calculated using the Eq.:

Degradation ratio (%) = (Initial dry weight -Dry weight/Initial dry weight) ×100 (2)

Each degradation test was performed five times (10).

3.4. Cell Culture Evaluations

3.4.1. BMMSCs Isolation and Characterization

All animal experiments have been approved by the animal ethics committees. BMMSCs were harvested from two-month-old male Wistar rats weighing about 200 g. The rats were sacrificed by ketamine/ xylazine overdose (50/125 mg.kg^{-1} Intraperitoneal), and stem cells were isolated from femoral bones. Obtained BMMSCs suspension was plated on 50 cm^2 tissue culture flasks containing 25 mL of DMEM/F12 supplemented with 15% (v/v) fetal bovine serum (FBS; Invitrogen), 100 IU.mL^{-1} penicillin, and 100 IU.mL^{-1} streptomycin in 5% (v/v) CO_2 at 37 °C (11).

3.4.2. Cell Seeding and Attachment on Freeze-Dried Scaffolds

After the BMMSCs reached 80% confluency, they were detached with trypsin–EDTA (0.25% trypsin and 0.1% EDTA) solution to obtain single-cell suspensions and were centrifuged at 1500 x g for 5 min. The 5×104 BMMSCs were seeded onto the top of freeze-dried scaffolds. After 3 days, cell-containing scaffolds were then fixed in 2.5% Glutaraldehyde solution at ambient temperature. Afterwards, the samples were washed three times with PBS and dehydrated in graded alcohols. Finally, the samples were sputter-coated with gold and studied using SEM (12).

3.4.3. Cell Viability Test

BMMSCs were incubated under the standard condition for 1, 3, and 5 days. Then, 60 µL of 5 mg.mL^{-1} stock MTT solutions was added to each well, and all plates were placed at 37 °C for 4 h. After that, the Formosan crystals were dissolved in dimethyl sulfoxide (DMSO). The final reading was analyzed by a spectrometer at a wavelength of 570 nm (12). The present investigation was used BMMSCs for the MTT reduction assay which is according to ISO 10993-5:2009 (standard numbers).

3.4.4. Neuronal Induction of BMMSCs

To induce neuronal differentiation, 1×10^4 BMMSCs from passage two were seeded on tissue culture plate (TCP) and both Gelatin/Collagen/Olibanum/ 1.5 wt% graphene oxide (GEL/COL/OL/ 1.5% GO) and Gelatin/ Collagen/Olibanum/ 3 wt% grapheme (GEL/COL/OL/ 3% GO) freeze-dried scaffolds and cultured in complete medium (DMEM containing with 10% FBS, 100 U.mL^{-1} penicillin, and 100 U.mL^{-1} streptomycin) for 2 days. The samples were pretreated with DMEM, 20 % FBS, 200 µM isobutylmethylxanthine, 100 µM 2-mercaptoethanol, 2 % B27, and 10 ng.mL^{-1} fibroblast growth factor 2 (FGF2) and culturing for 1day at 37 °C and 5 % CO_2. Neural differentiation medium containing with DMEM/F12 (1:1), 100 ng.mL^{-1} of Shh, 0.01 ng.mL^{-1} RA, and 0.2 % B27 was then added to each well for 7 days. The differentiation medium was then changed with media containing DMEM/F12, 0.2 % B27, and 200 ng.mL brain-derived neurotrophic factor (BDNF) for 7 days (13).

3.4.5. Immunohistochemical Analysis

Detection of proteins expressed on cells is performed using labelled antibodies. Cell-containing scaffolds were fixed for 4 h at 4 °C in 300 µL Zamboni's fixative (0.2% picric acid in 0.1 M phosphate buffer saline and 2% paraformaldehyde), immersed in 30% sucrose in 0.1 M PBS solution for 12 h, embedded in OCT mounting medium (Sakura Finetechnical, Tokyo, Japan), and sectioned at 10 µM thickness using a cryostat at -20 °C. Then the samples were deparaffinized with xylene for 5 min, gradually rehydrated with 100%, 95%, 80%, and 70% graded ethanol (each for 5 min), and then permeabilized with 0.1% Triton X-100 in PBS (Sigma-Aldrich, USA) for 20 min, and blocked with 10% serum in PBS at room temperature. Prepared sections were then incubated at 4 °C for 20 h with primary antibodies: Islet-1 (ab20670; Abcam, Cambridge, UK, 1:1000) and Tuj-1 (ab18207; Abcam, Cambridge, UK, 1:200). Samples were rinsed 4 times in PBS, incubated with Alexa Fluor

Table 1. Sequences of primers used for real-time PCR

Gene	Product Length(bp)	Primer sequnces (5' to 3')
Chat	240	F: AGCCTGAACGGAGCCAAT R: GGCGAGATGGCCTTGGGTT
Pax6	130	F: CACCCGCCCTGGTTGGTAT R: AGCTGCAGCCGCATTTGA
HB9	245	F: GCACAGGCAGCTCTCTACGG R: GATTGCGCCTGGGAGCTGAA
Nestin	160	F: CTCCAGGAGCGCAGAGAAG R: CAGTTGCTGCCCACCTTCCA
Islet-1	250	F: TGGGAGACATGGGCGATCCA R: TGCTGCACTTGGCGCATTTG
NF-H	190	F: GCAGGAAGAGTGCGGCTACC R: GCGTACTCTGCACCGTGTGT
GAPDH	230	F:GCCTGGAGAAACCTGCCAA R: ACCACCCTGTTGCTGTAG

488 Goat Anti-Rabbit IgG H&L (ab150077; Abcam, Cambridge, UK, 1:500) and Alexa Fluor 647 Goat Anti-Rabbit IgG H&L (ab150079; Abcam, Cambridge, UK, 1:500) secondary antibodies for 2 h. Sections were washed four times with PBS, counterstained with DAPI and studied under a fluorescence microscope (Optika, XDS-3FL, Italy) (13). Expression of islet-1 and TUJ1 biomarkers compared with control, GEL/COL/OL, and GEL/COL/OL/1.5% GO freeze-dried scaffolds were evaluated. Each Positive ratio test was performed three times.

3.4.6. Real-Time PCR

To determine the difference between the messenger RNA expression levels of Choline acetyltransferase (Chat), Paired type homobox 6 (Pax6), HB9/HLXB9 (HB9), Nestin, Islet-1, and neurofilament-H (NF-H) in differentiated cells, real-time PCR was performed. The oligonucleotide primer sequences (**Table 1**) were designed for each sample using Oligo7, GeneRunner, and BioEdit softwares. The total RNA was extracted applying Qiagen RNeasy Plus Mini Kit, DNAse 1 treatment was applied (Ambion, Country), and isolated RNA was reverse-transcribed to random hexamer primed cDNA by TAKARA cDNA synthesis kit. GAPDH is the internal reference (14).

3.5. Statistical Analysis

The results were analyzed by GraphPad Prism 8 (GraphPad Prism 8.2.1) using one-way ANOVA test and paired t-Test. The obtained results were expressed as mean ± standard deviation in three replications. Values of *P<0.05, **P<0.01, and ***P<0.001 were considered statistically significant.

4. Results

4.1. Scaffold Morphology

Interconnected porous scaffolds should imitate extracellular microenvironment to promote cellular migration, penetration, and proliferation. Images reveal the different porosities are constructed wall-like, and a suitable porous structure was formed (**Fig. 1A**). Results denote that, for the GO with different concentrations, there is negligible impact on the morphology structure, distribution of pore interconnectivity (arrows), and pore size in the fabricated scaffolds. The SEM micrographs obtained from the freeze-dried scaffolds show that the pore size is increased in GEL/COL/OL/GO scaffolds compared with GO-free scaffolds. The porosity and pore size of freeze-dried scaffolds are shown in **Table 2**.

4.2. FTIR

The FTIR spectra of the GO and GEL/COL/OL/GO are shown in **Figure 1B**. In the case of OL, the C=O and OH stretching bands are detected at 1600 cm^{-1} (15) and at approximately 3600 cm^{-1} , respectively (16). Investigation of GEL in GEL/COL/OL/GO scaffolds shows that the absorption bands at 1538 and 1650 cm^{-1} attributed to amide II and amide me stretching vibrations, respectively (17). The absorption spectrum at 1500 cm^{-1} is related to hydroxyproline

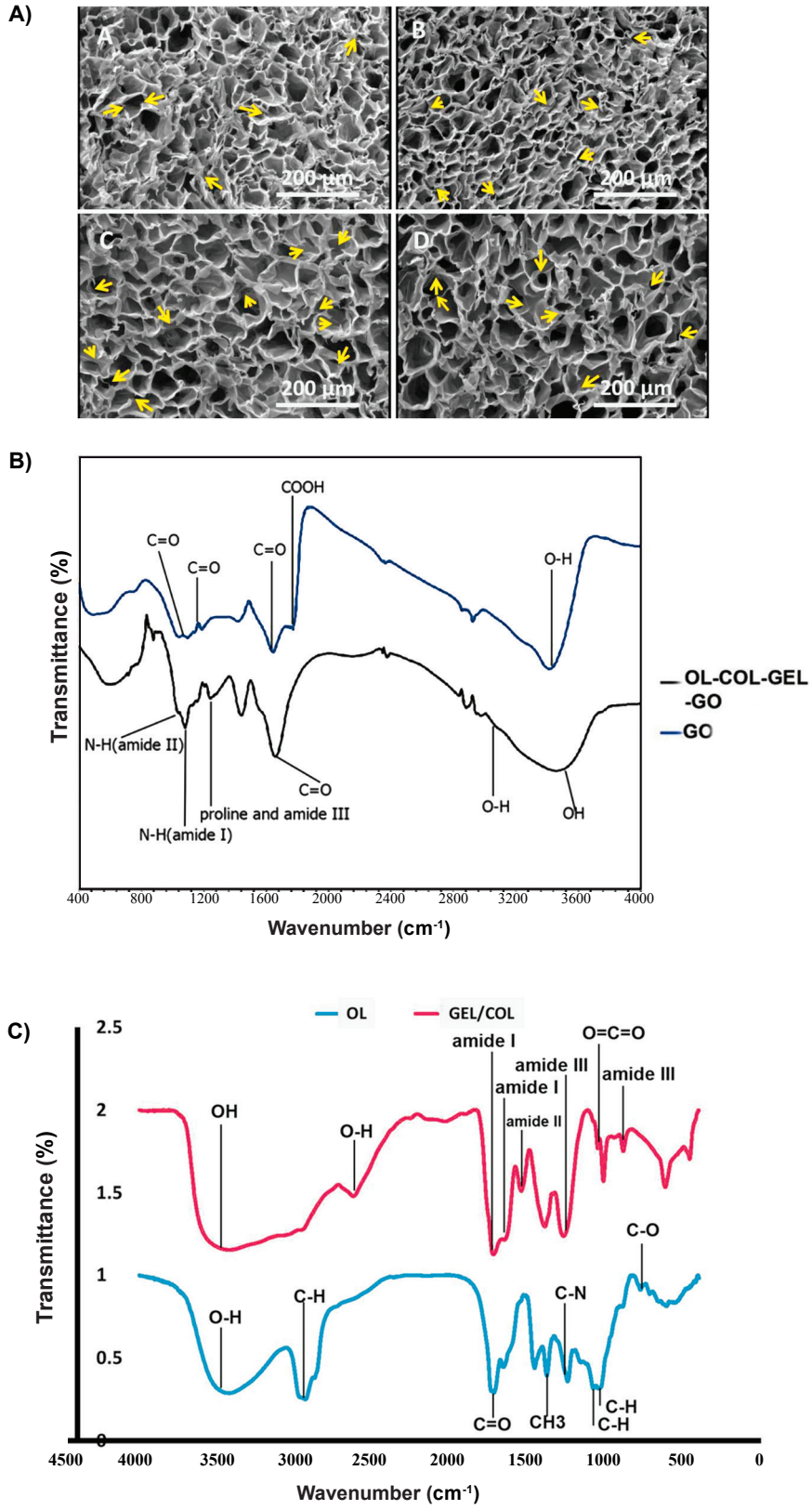

Figure 1. A) SEM micrographs of freeze-dried scaffolds **A:** GEL/COL, **B:** GEL/COL/OL, **C:** GEL/COL/OL/ 1.5% GO, **D:** GEL/COL/OL/ 3% GO). Arrow indicates pore interconnectivity in each scaffold. **(B, C)** FTIR spectra of raw materials (GO and OL) and freeze-dried scaffolds (GEL/COL/OL and GEL/COL/OL/GO).

Table 2. Morphological characteristics of freeze-dried scaffolds

Composition	Porosity (%)	Pore Size (µm)
GEL/COL	68	39±10
GEL/COL/OL	73	44±10
GEL/COL/OL/1.5% GO	86	62±10
GEL/COL/OL/3% GO	88	65±10

and pyrrolidine ring vibrations of proline in both GEL and COL samples, and amide III group is assigned to the presence of the native COL in GEL/COL/OL/GO freeze-dried scaffolds (18). The stretching vibration at 3500 cm^{-1} and 3000 cm^{-1} (O–H vibration) are characteristic of COL structure (19). OH stretching vibration around 3340 cm^{-1} is observed, indicating the presence of GO. Two absorption peaks showing at 1630 cm^{-1} and 1730 cm^{-1}, related to C=O and COOH stretching bands in GO, respectively (20). The peaks at 1044 cm^{-1} and 1226 cm^{-1} attribute to the bending mode of C=O in GO (21) (**Fig. 1B)**. The FTIR of crude OL resin assigned bands at 734 cm^{-1}, 1051 cm^{-1}, 1060 cm^{-1}, 1245 cm^{-1}(22), 1380 cm^{-1} (23), 1455 cm^{-1} (C–H stretching)(24), 1716 cm^{-1} (C=O stretching), 2943 cm^{-1} (C–H stretching), and 3366 cm^{-1} (O–H stretching) (22). The band at 734 cm^{-1} is related to the C–O stretching vibration responsible for aldehydes. The peak at 1051 cm^{-1} corresponds to the C–H stretching frequency. The bands at 1060 cm^{-1} and 1245 cm^{-1} attribute to the bending mode of C–N stretching frequency. The spectrum showed absorption bands at 1380 cm^{-1} for -CH3 stretching vibration. The FTIR spectrum of GEL/COL scaffolds assigned to absorption peaks at 880 cm^{-1} (amide III of hydroxyproline) (25), 1037 cm^{-1} (O=C=O vibration) (26), 1270 cm^{-1} (Amide III) (27), 1540 cm^{-1} (amide II) (28), 1722 cm^{-1} (amide I) (29), 2623 cm^{-1} (O-H stretch), and 3421 cm^{-1} (O-H stretch) (30) (**Fig. 1C**).

4.3. Compressive Strength Behavior

Figure 2A compares the compressive strength values of GEL/COL and GEL/COL/OL (GO-free) scaffolds and GEL/COL/OL/GO scaffolds with different concentrations of GO (A: 1.5 wt%, B: 3 wt. %), prepared by the freeze-dried method. The strength values of the GEL/COL/OL/ 1.5% GO and GEL/COL/OL/3% GO scaffolds were 2.86 ± 0.05 MPa and 2.92 ± 0.04 MPa, respectively, which were significantly different from the GEL/COL (0.95±0.04 MPa) and GEL/COL/OL scaffolds (0.99±0.05 MPa). Mechanical behavior was affected by GO loading in the freeze-dried scaffolds. Scaffolds containing GO shows higher mechanical properties compared with GO-free scaffolds.

4.4. Water Absorption

The swelling ratio shows water uptake capability which could be useful for the biological efficiency of scaffolds. The water absorption ability of polymeric scaffolds after 1 day of incubation was 1173, 1172, 1182, and 1186 for GEL/COL, GEL/COL/OL, GEL/COL/OL/ 1.5% GO, and GEL/COL/OL/3% GO scaffolds, respectively **Figure 2B.** The water absorption was progressed until the end of the experiment. Due to the high hydrophilicity of GO, its presence promotes the water absorption of the fabricated scaffold.

4.5. Degradation Test

The degradability of scaffolds is the chemical breakdown of substances in the body that results in altered physical and chemical properties. The results of percent reduction of scaffold mass over the 4 weeks are shown in **Figure 2C.** The results denoted that by increasing the amount of GO content from 1.5 wt% to 3 wt%, degradation in GEL/COL/OL/GO freeze-dried scaffolds is increased. Degradation of the GEL/COL/OL/GO scaffolds provides the conditions for tissue regeneration and the replacement of scaffold with regenerated tissue.

4.6. BMMSCs Isolation

Cells spread on TCP showed spindle-shaped morphology after 3 days. After nearly a week of initial plating, they proliferated into clusters. These cells were mainly spindle and rounded shape, or large flattened morphology. BMMSCs at the third passage appeared as morphologically homogeneous fibroblast-like cells and proliferated rapidly on culture plates (**Fig. 3A**).

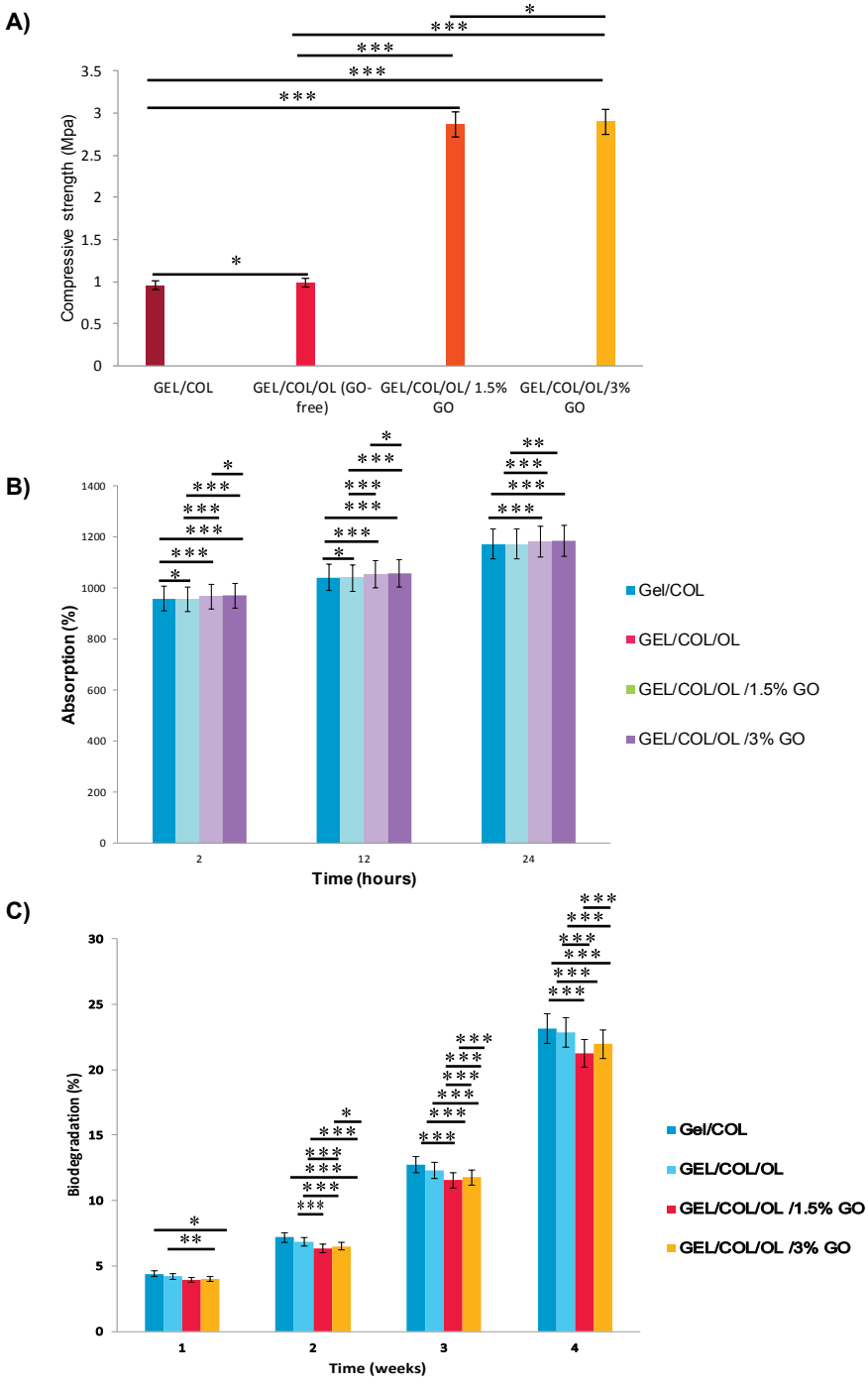

Figure 2. A) Compressive strength of scaffolds. **B)** Water absorption of scaffolds with different concentration of GO. **C)** Degradability of different scaffolds. (*P<0.05, **P<0.01, ***P<0.001).

4.7. Cell Seeding and Attachment on Freeze-Dried Scaffolds

SEM micrographs of cell adhesion on freeze-dried scaffolds after 72 h of culture was revealed in **Figure 3B** (**A-H**). After culturing the same number of BMMSCs on freeze-dried scaffolds, SEM images indicated spread and attachment of BMMSCs on the freeze-dried scaffolds, but higher BMMSCs proliferation on GEL/COL/OL /1.5% GO scaffolds (**Fig. 3B (E , F))** were detected. These results reveal a considerable interaction of BMMSCs with GEL/COL/OL /1.5% GO freeze-dried scaffolds.

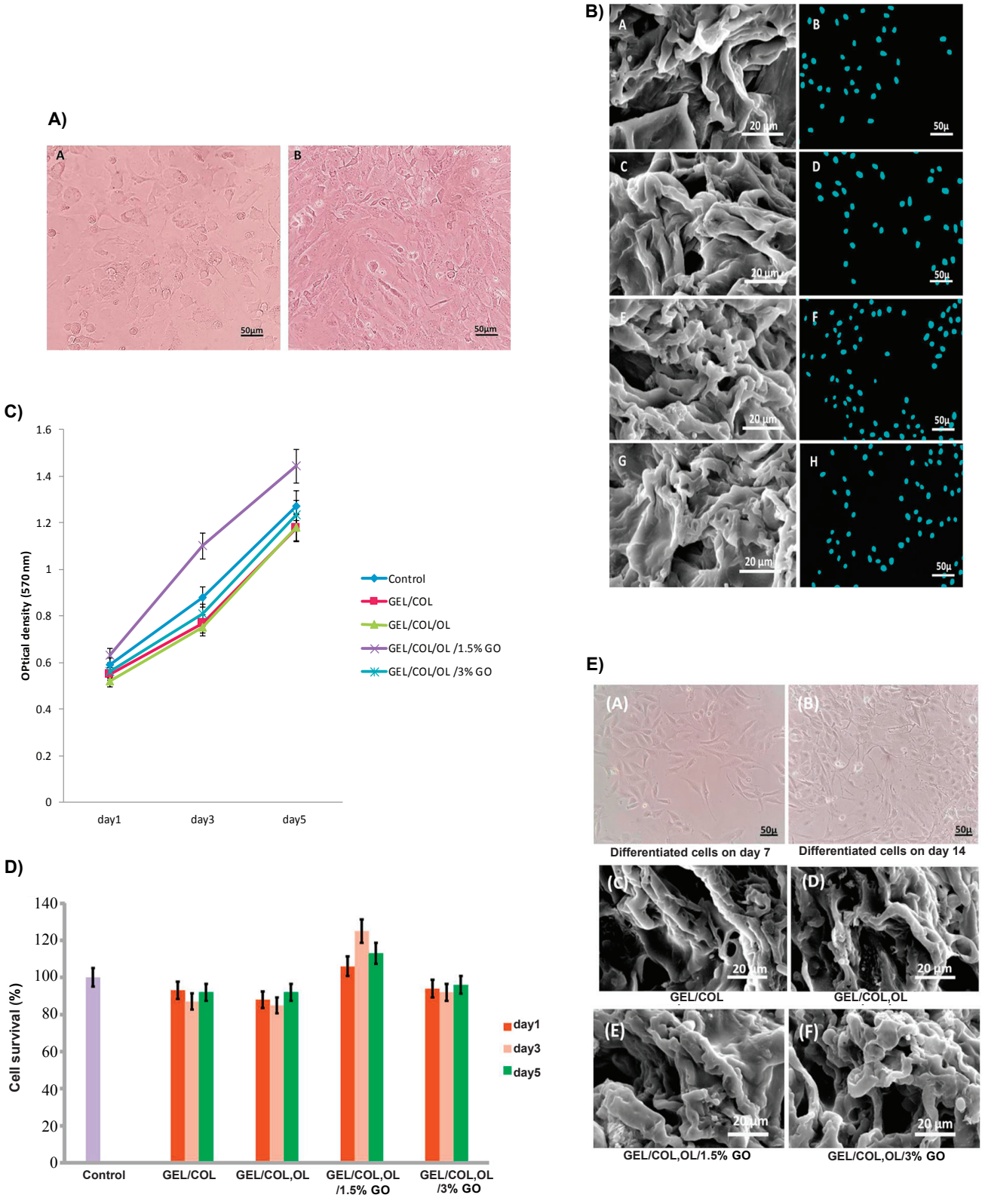

Figure 3. A) BMMSCs isolation **A:** 24h after isolation, cells spread to tissue culture plate, **B:** spindle-shaped morphology after 3 days). **B)** SEM images and DAPI stained nucleus of BMMSCs on freeze-dried scaffolds. **(C** and **D)** MTT test (*P<0.05, **P<0.01, ***P<0.001) (n=3). **E)** Morphological feature of neuron-like cells induced from BMMSCs after the neuronal induction.

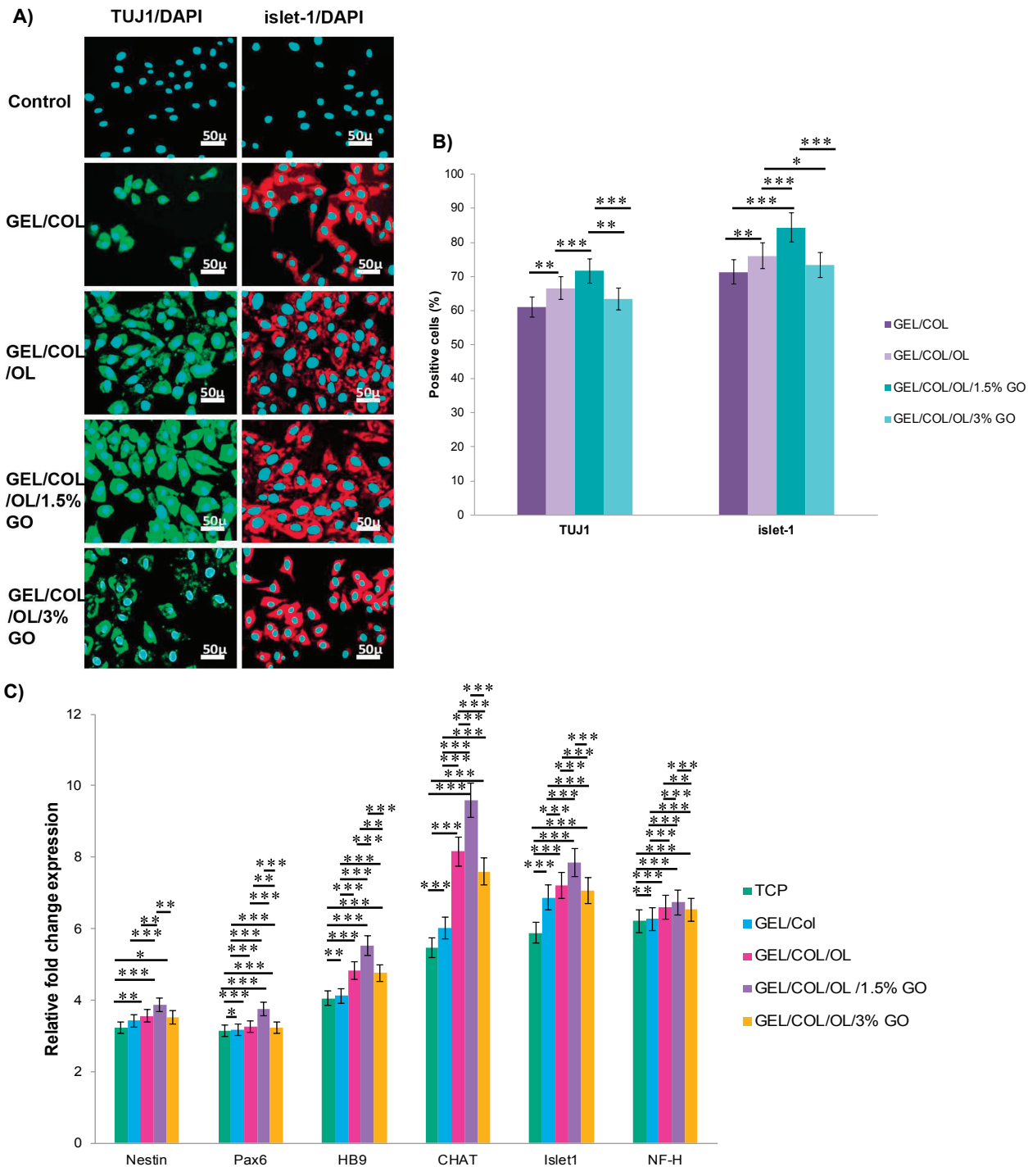

Figure 4. A) Immunohistochemical images of differentiated cells. **B**) Expression of neuronal biomarkers compared with other groups. **C**) Quantitative assessment of the expression of neuron-like cells markers in differentiated BMMSCs. (*P<0.05; **P<0.01, ***P<0.001, n=3, mean ± SD).

4.8. Cell Viability Test

Cell viability of BMMSCs cultured on freeze-dried scaffold at the concentration of 1.5% GO was significantly higher than scaffolds at the concentrations of 3% GO, Gel/COL, GEL/COL/OL, and TCP **(Fig. 3C, 3D)**. Only freeze-dried scaffold at the concentration of 1.5% GO provoked higher cell proliferation than TCP culture **(Fig. 3C, 3D)**. The result of BMMSCs viability analysis for 24 h indicated that there is a higher proliferation in two dimensional (2D) on TCP than in BMMSCs cultured on

the GEL/COL/OL /3% GO scaffold **(Fig. 3C, 3D)**. At days 3 and 5 of post culturing, the GEL/COL/OL /1.5% GO freeze-dried scaffold revealed a higher impact on the increment in the cell viability than the TCP. The cell viability results after 5 days of incubation showed the significant biocompatibility of GEL/COL/OL /1.5% GO freeze-dried scaffold for BMMSCs attachment and proliferation. These data are in accordance with ISO standards (10993-5).

4.9. Neuronal Induction of Bone Marrow Mesenchymal Stem Cells

To detect neuronal induction, the treating BMMSCs were assessed daily by a phase-contrast microscope. After 1 day, the adherent BMMSCs was spindle-like cells. These cells were then induced by neural-signaling molecules, RA, Shh, etc., by 7 days, fibroblast-shaped cells were bipolar appearance and become elongated cells. Axon-like cytoplasmic processes elongated extremely and interconnected with each other during the second week of neuronal induction **(Fig. 3E)**. Untreated BMMSCs group denoted no significant morphological characterization as a control group that presented a spindle fibroblast-like cell.

4.10. Immunohistochemical Analysis

In the case of motor neuron-specific proteins (islet-1) and early neural marker (TUJ1), they were expressed in three-dimensional (3D) culture samples compared with the control group (Untreated BMMSCs) (**Fig. 4A**). Immunohistochemical analysis denoted that differentiated BMMSCs were positive for islet-1 and TUJ1 after 14 days post-neural inductions. Expression of the neuronal markers in differentiated neural-like cells from BMMSCs is denoted in **Figure 4B.**

4.11. Real-Time PCR Analysis

Investigation of RNA expression in differentiated cells was performed 14 days' post-neural induction. The induction of BMMSCs with RA and Shh resulted in the increase of *Chat*, *Pax6*, *Hb-9*, *Nestin*, *Islet-1*, and *NF-H* in 2D and 3D culture samples at second week post-induction. In this study, an increment in the expression of Chat and Islet-1 messenger RNA levels in the neuronal induction cells cultured on freeze-dried scaffolds in comparison with BMMSCs cultured in TCP was shown.

Our results denoted that expression of neuron-specific markers (*Chat, Pax6, Hb-9, Nestin, Islet-1*, and *NF-H*) significantly upregulated ($P<0.05$, $P<0.01$, $P<0.001$) in cells differentiated on GEL/COL/OL/1.5% GO scaffolds compared with GEL/COL, GEL/COL/OL, GEL/COL/OL/3% GO scaffolds and TCP at day 14 post-induction (**Fig. 4C**). These results revealed the positive role of 1.5% GO and 3D culture in neural induction.

5. Discussion

In this study, we assessed the differentiation of BMMSCs in well-defined biochemical and mechanical microenvironments. BMMSCs can differentiate into multiple cell lines when they exposed to a substrate under suitable conditions. Anchorage-dependent cells need appropriate adhesion to stroma in order to attach, proliferate, and support cellular functions. In our study, good BMSC adhesion can be found for GEL/COL/OL/GO freeze-dried scaffolds (**Fig. 3B**), which is an essential requirement in tissue engineering. Suitable cell adhesion on scaffolds, consistent with cell viability for BMMSCs, should mainly be attributed to unique surface characteristics of GO material itself. The wrinkles and ripples on the surface of scaffold likely resulted in an improved mechanical interlocking with cells and therefore better bonding, for surface structure of the material can particularly impact the cell adhesion (31). Culturing the isolated BMMSCs on the GEL/COL/OL/GO freeze-dried scaffolds confirmed the suitable behavior of GO in the biocompatibility of the fabricated scaffolds for cellular adhesion, spreading and proliferation properties. Their findings indicated that the application of GO can be a promising biomaterial for regenerative engineering like nervous tissue. In this study, results of SEM and MTT tests showed that the GEL/COL/OL/ 1.5% GO freeze-dried scaffolds have a higher effect on the cell viability. According to the SEM micrographs, proliferation of the cultured cells was better on the GEL /COL /OL /1.5% GO scaffolds due to larger pores and proportion of cell sizes and pores for attachment. Better proliferation of BMMSCs on GEL /COL /OL /1.5% GO samples are a sign of viability and MTT results (**Fig. 3C)** confirmed this reality. Ghorbani *et al* (2020) demonstrated that the OL /COL /GEL freeze-dried scaffolds had a good oriented microstructure ended to favorable cellular interaction (32). In the immunostaining, BMMSCs were well-improved attachment on the scaffolds during the treatment period; the majority of neural induction cells were expressed

neural biomarkers. These data indicate that MSCs seem more differentiated into neural progenitor cells toward glial progenitor cells on the nanostructure, similar to the result of Guo *et al* (33). As shown in **Figure 4C**, expression of neuron-specific markers (*Islet-1, Pax6, Nestin, Hb-9*, and *Chat*) significantly upregulated ($P<0.001$) in cells differentiated on freeze-dried scaffolds compared with TCP and control group at day 14 post-induction. These results show that GEL /COL /OL /1.5% GO freeze-dried scaffolds are approporate for the BMMSCs neuronal differentiation, and it also revealed that this structure is a suitable construction for the increment of BMMSCs differentiation into neuron-like cells. Several inducers, including neurotrophic factor, chemical inducer, and herbal extracts, have been indicated to be able to differentiate MSCs into neuron expressing specific surface markers of neural cells (34). Ghorbani *et al* (2020) confirmed that OL, an active ingredient in traditional Iranian herbal medicine, could effectively increase BMMSCs to differentiate into neurons in vitro. Furthermore, the optimal concentration of OL for acquiring these inductive impacts was determined to be 1%. Various inducers have several mechanisms for promoting neuronal cell differentiation. When OL was used as a neuronal inducer, BMMSCs showed process-like extensions and multipolar cell bodies, and expressed neural-signaling molecules. These results denote that BMMSCs differentiate into neuron-like cells both functionally and morphologically (35). According to some data obtained by animal studies, OL and its component, have obvious positive effects on neurodegenerative diseases (36). It was noticed in many investigations that OL inhibits inflammation in various inflammatory diseases by clearly inhibiting 5-lipoxygenase enzyme, blocking leukotriene synthesis, and preventing glycosaminoglycan production (37). Marefati *et al* showed that OL could promote synaptic plasticity impairment through anti-oxidant and anti-inflammation effects (38). Zhou *et al* showed a decrease of inflammatory responses of microglia, astrocytes, and infiltrated macrophages in OL implanted scaffolds into the striatum of adult rats (39). It was also recommended that active constituents of OL extract could be useful in repairing a variety of models of memory impairment and cognitive dysfunction caused by seizure (40), stroke (41), and Alzheimer's disease (42). However, its effect on stem cells should have further investigations to clarify its mechanism on the induction of MSCs to differentiate into neural cells. As a pilot study, this investigation has successfully verified the effectiveness of a GEL/ COL/OL/GO scaffold and BMMSCs for neural differentiation. Such observed results should be further studied in appropriate in vitro and in vivo models to understand possible mechanisms involved. Well-characterized herbal extracts and other biomaterials that result in increased rates of tissue repair and regeneration may be used in both tissue engineering for replacement therapy and stem cell therapy, where the use of vesicles and scaffolds with improved attaching and proliferative characteristics could be very helpful in the latter. Although the clinical application of vegetal extracts is still in evaluation due to the complexity and variability of bioactive components, standardized herbal extract preparations will increase their use in the clinical context.

6. Conclusion

In this investigation, we have denoted that olibanum extract/graphene (OL/GO) incorporated with gelatin/ collagen (GEL/COL) scaffolds which fabricated by freeze-dried method have the suitable candidate to improve stem cells differentiation into the neuron-like cells.

Acknowledgment

We would like to acknowledge and extend our deepest gratitude to Ali Zamanian in Materials and Energy Research Center for his technical help and useful comments.

Conflict of interest

The authors whose names are listed certify that they have NO affiliations with or involvement in any organization or entity with any financial interest, or non-financial interest in the subject matter or materials discussed in this manuscript.

References

1. Lee WC, Loh KP, Lim CT. When stem cells meet graphene: Opportunities and challenges in regenerative medicine. *Biomaterials*. 2018;**155**:236-250. doi:10.1016/j.biomaterials.2017.10.004.
2. Pan Y, Liu F, Qi X, Hu Y, Xu F, Jia H. Nerve Growth Factor Changes and Corneal Nerve Repair after Keratoplasty. *Optom Vis Sci*. 2018;**95**(1):27-31. doi:10.1097/opx.0000000000001158.
3. Chico B, Pérez-Maceda BT, San José S, Escudero ML, García-Alonso MC, Lozano RM. Corrosion Behaviour and J774A. 1 Macrophage Response to Hyaluronic Acid Functionalization of Electrochemically Reduced Graphene Oxide on Biomedical

Grade CoCr. *Metals*. 2021;**11**(7):1078. doi:10.3390/met1107 1078.
4. Di Stefano V, Schillaci D, Cusimano MG, Rishan M, Rashan L. In vitro antimicrobial activity of frankincense oils from Boswellia sacra grown in different locations of the Dhofar region (Oman). *Antibiotics*. 2020;**9**(4):195. doi:10.3390/ antibiotics9040195.
5. Kebebe D, Belete A, Gebre-Mariam T. Evaluation of two olibanum resins as rate controlling matrix forming excipients in oral sustained release tablets. *Ethiop Pharm J*. 2010;**28**:95-109. doi:10.4314/epj.v28i2.4.
6. Lee KP, Park ES, Kim DE, Park IS, Kim JT, Hong H. Artemisinin attenuates platelet-derived growth factor BB-induced migration of vascular smooth muscle cells. *Nutr Res Pract*. 2014;**8**(5):521-525. doi:10.4162/nrp.2014.8.5.521.
7. Meyer M, Morgenstern B. Characterization of gelatine and acid soluble collagen by size exclusion chromatography coupled with multi angle light scattering (SEC-MALS). *Biomacromolecules*. 2003;**4**(6):1727-1732. doi:10.1021/bm03 41531.
8. Aidun A, Zamanian A, Ghorbani F. Novel bioactive porous starch-siloxane matrix for bone regeneration: Physicochemical, mechanical, and in vitro properties. *Biotechnol Appl Biochem*. 2019;**66**(1):43-52. doi:10.1002/bab.1694.
9. Selvakumar G, Lonchin S. Fabrication and characterization of collagen-oxidized pullulan scaffold for biomedical applications. *Int J Biol Macromol*. 2020;**164**:1592-1599. doi:10.1016/j.ijbiomac.2020.07.264.
10. Honda M, Hariya R, Matsumoto M, Aizawa M. Acceleration of Osteogenesis via Stimulation of Angiogenesis by Combination with Scaffold and Connective Tissue Growth Factor. *Materials (Basel)*. 2019;**12**(13). doi:10.3390/ma12132068.
11. Li C, Wang F, Zhang R, Qiao P, Liu H. Comparison of Proliferation and Osteogenic Differentiation Potential of Rat Mandibular and Femoral Bone Marrow Mesenchymal Stem Cells In Vitro. *Stem Cells Dev*. 2020;**29**(11):728-736. doi10.1089/scd.2019.0256.
12. Grenier J, Duval H, Barou F, Lv P, David B, Letourneur D. Mechanisms of pore formation in hydrogel scaffolds textured by freeze-drying. *Acta Biomater*. 2019;**94**:195-203. doi:10.1016/j.actbio.2019.05.070.
13. Nagel J, Wollner S, Schurmann M, Brotzmann V, Muller J, Greiner JF*, et al.* Stem cells in middle ear cholesteatoma contribute to its pathogenesis. *Sci Rep*. 2018;**8**(1):6204. doi:10.1038/s41598-018-24616-4.
14. Mahmoudi E, Mozhgani SH, Sharifinejad N. The role of mycobiota-genotype association in inflammatory bowel diseases: a narrative review. *Gut Pathog*. 2021;**13**(1):31. doi:10.1186/s13099-021-00426-4.
15. Bruni S, Guglielmi V. Identification of archaeological triterpenic resins by the non-separative techniques FTIR and 13C NMR: the case of Pistacia resin (mastic) in comparison with frankincense. *Spectrochim Acta A Mol Biomol Spectrosc*. 2014;**121**:613-622. doi:10.1016/j.saa.2013.10.098.
16. Velusamy P, Su CH, Venkat Kumar G, Adhikary S, Pandian K, Gopinath SC*, et al.* Biopolymers Regulate Silver Nanoparticle under Microwave Irradiation for Effective Antibacterial and Antibiofilm Activities. *PLoS One*. 2016;**11**(6):e0157612. doi:10.1371/journal.pone.0157612.
17. Fiorani A, Gualandi C, Panseri S, Montesi M, Marcacci M, Focarete ML*, et al.* Comparative performance of collagen nanofibers electrospun from different solvents and stabilized by different crosslinkers. *J Mater Sci Mater Med*. 2014;**25**(10):2313-2321. doi:10.1007/s10856-014-5196-2.
18. Li Y, Chen M, Zhou W, Gao S, Luo X, Peng L*, et al.* Cell-free 3D wet-electrospun PCL/silk fibroin/Sr(2+) scaffold promotes successful total meniscus regeneration in a rabbit model. *Acta Biomater*. 2020;**113**:196-209. doi:10.1016/j. actbio.2020.06.017.
19. Sousa RO, Alves AL, Carvalho DN, Martins E, Oliveira C, Silva TH*, et al.* Acid and enzymatic extraction of collagen from Atlantic cod (Gadus Morhua) swim bladders envisaging health-related applications. *J Biomater Sci Polym Ed*. 2020;**31**(1):20-37. doi: 10.1080/09205063.2019.1669313.
20. Karimi N, Kharaziha M, Raeissi K. Electrophoretic deposition of chitosan reinforced graphene oxide-hydroxyapatite on the anodized titanium to improve biological and electrochemical characteristics. *Mater Sci Eng C Mater Biol Appl*. 2019;**98**:140-152. doi:10.1016/j.msec.2018.12.136.
21. Sametband M, Kalt I, Gedanken A, Sarid R. Herpes simplex virus type-1 attachment inhibition by functionalized graphene oxide. *ACS Appl Mater Interfaces*. 2014;**6**(2):1228-1235. doi:10.1021/am405040z.
22. Al-Dahmash ND, Al-Ansari MM, Al-Otibi FO, Singh AR. Frankincense, an aromatic medicinal exudate of Boswellia carterii used to mediate silver nanoparticle synthesis: Evaluation of bacterial molecular inhibition and its pathway. *J Drug Deliv Sci Technol*. 2021;**61**:102337. doi:10.1016/j. jddst.2021.102337.
23. Sharma T, Jana S. Bioassay-guided isolation, identification, and evaluation of anti-inflammatory activity of β-boswellic alcohol and 3-o-acetyl-11-hydroxy-β-boswellic acid from the leaves of Boswellia serrata. *Pharmacogn Mag*. 2020;**16**(69):264.
24. Tambe A, Pandita N, Kharkar P, Sahu N. Encapsulation of boswellic acid with β-and hydroxypropyl-β-cyclodextrin: Synthesis, characterization, in vitro drug release and molecular modelling studies. *J Mol Struct*. 2018;**1154**:504-510. doi:10.1016/j.molstruc.2017.10.061.
25. Xu C, Wang Y. Chemical composition and structure of peritubular and intertubular human dentine revisited. *Arch Oral Biol*. 2012;**57**(4):383-391. doi:10.1016/j. archoralbio.2011.09.008.
26. Rajasree SR, Gobalakrishnan M, Aranganathan L, Karthih M. Fabrication and characterization of chitosan based collagen/ gelatin composite scaffolds from big eye snapper Priacanthus hamrur skin for antimicrobial and anti oxidant applications. *Mater Sci Eng C*. 2020;**107**:110270. doi:10.1016/j. msec.2019.110270.
27. Goheen SC, Lis LJ, Kauffman JW. Raman spectroscopy of intact feline corneal collagen. *Biochim Biophys Acta*. 1978;**536**(1):197-204. doi:10.1016/0005-2795(78)90065-x.
28. Hashim D, Man YC, Norakasha R, Shuhaimi M, Salmah Y, Syahariza Z. Potential use of Fourier transform infrared spectroscopy for differentiation of bovine and porcine gelatins. *Food Chem*. 2010;**118**(3):856-860. doi:10.1016/j. foodchem.2009.05.049.
29. Cebi N, Durak MZ, Toker OS, Sagdic O, Arici M. An evaluation of Fourier transforms infrared spectroscopy method for the classification and discrimination of bovine, porcine and fish gelatins. *Food Chem*. 2016;**190**:1109-1115. doi:10.1016/j. foodchem.2015.06.065.
30. Ahmad Ruzaidi DA, Mahat MM, Mohamed Sofian Z, Nor

Hashim NA, Osman H, Nawawi MA*, et al.* Synthesis and Characterization of Porous, Electro-Conductive Chitosan–Gelatin–Agar-Based PEDOT: PSS Scaffolds for Potential Use in Tissue Engineering. *Polymers*. 2021;**13**(17):2901. doi:10.3390/polym13172901.

31. Fon D, Zhou K, Ercole F, Fehr F, Marchesan S, Minter MR*, et al.* Nanofibrous scaffolds releasing a small molecule BDNF-mimetic for the re-direction of endogenous neuroblast migration in the brain. *Biomaterials*. 2014;**35**(9):2692-2712. doi:10.1016/j.biomaterials.2013.12.016.
32. Ghorbani F, Zamanian A, Kermanian F, Shamoosi A. A bioinspired 3D shape olibanum-collagen-gelatin scaffolds with tunable porous microstructure for efficient neural tissue regeneration. *Biotechnol Prog*. 2020;**36**(1):e2918. doi:10.1002/btpr.2918.
33. Guo W, Qiu J, Liu J, Liu H. Graphene microfiber as a scaffold for regulation of neural stem cells differentiation. *Sci Rep*. 2017;**7**(1):5678. doi:10.1038/s41598-017-06051-z.
34. Spelman K, Aldag R, Hamman A, Kwasnik EM, Mahendra MA, Obasi TM*, et al.* Traditional herbal remedies that influence cell adhesion molecule activity. *Phytother Res*. 2011;**25**(4):473-483. doi: 10.1002/ptr.3350.
35. Hosseini-sharifabad M, Esfandiari E. Effect of Boswellia serrata gum resin on the morphology of hippocampal CA1 pyramidal cells in aged rat. *Anat Sci Int*. 2015;**90**(1):47-53. doi:10.1007/s12565-014-0228-z.
36. Morgese MG, Bove M, Francavilla M, Schiavone S, Dimonte S, Colia AL*, et al.* Sublingual AKBA Exerts Antidepressant Effects in the Abeta-Treated Mouse Model. *Biomolecules*. 2021;**11**(5). doi:10.3390/biom11050686.
37. Marefati N, Beheshti F, Memarpour S, Bayat R, Naser Shafei M, Sadeghnia HR*, et al.* The effects of acetyl-11-keto-beta-boswellic acid on brain cytokines and memory impairment induced by lipopolysaccharide in rats. *Cytokine*. 2020;**131**:155107. doi:10.1016/j.cyto.2020.155107.
38. Wang Y, Sun Y, Wang C, Huo X, Liu P, Wang C*, et al.* Biotransformation of 11-keto-beta-boswellic acid by Cunninghamella blakesleana. *Phytochemistry*. 2013;**96**:330-336. doi:10.1016/j.phytochem.2013.07.018.
39. Zhou K, Motamed S, Thouas GA, Bernard CC, Li D, Parkington HC*, et al.* Graphene Functionalized Scaffolds Reduce the Inflammatory Response and Supports Endogenous Neuroblast Migration when Implanted in the Adult Brain. *PLoS One*. 2016;**11**(3):e0151589. doi:10.1371/journal.pone.0151589.
40. Amri IA, Mabood F, Kadim IT, Alkindi A, Al-Harrasi A, Al-Hashmi S*, et al.* Evaluation of the solubility of 11-keto-beta-boswellic acid and its histological effect on the diabetic mice liver using a novel technique. *Vet World*. 2021;**14**(7):1797-1803. doi:10.14202/vetworld.2021.1797-1803.
41. Miao XD, Zheng LJ, Zhao ZZ, Su SL, Zhu Y, Guo JM*, et al.* Protective Effect and Mechanism of Boswellic Acid and Myrrha Sesquiterpenes with Different Proportions of Compatibility on Neuroinflammation by LPS-Induced BV2 Cells Combined with Network Pharmacology. *Molecules*. 2019;**24**(21). doi:10.3390/molecules24213946.
42. Mohamed TM, Youssef MAM, Bakry AA, El-Keiy MM. Alzheimer's disease improved through the activity of mitochondrial chain complexes and their gene expression in rats by boswellic acid. *Metab Brain Dis*. 2021;**36**(2):255-264. doi:10.1007/s11011-020-00639-7.